



# Accurate analytical non-gravitational force model for precise orbit determination of QZS-1, 2, and 4

Satoshi Ikari<sup>1</sup> · Kyohei Akiyama<sup>2</sup> · Yuki Igarashi<sup>2</sup> · Kaori Kawate<sup>2</sup> · Toshitaka Sasaki<sup>2</sup> · Yasuyuki Watanabe<sup>3</sup> · Takuji Ebinuma<sup>4</sup> · Shinichi Nakasuka<sup>1</sup>

Received: 22 March 2023 / Accepted: 26 July 2023 / Published online: 24 August 2023  
© The Author(s), under exclusive licence to Springer-Verlag GmbH Germany, part of Springer Nature 2023

## Abstract

We propose an accurate analytical non-gravitational force model of QZS-1, 2, and 4 for a precise orbit determination of these satellites. To construct an accurate disturbance model, we used a high-fidelity satellite geometry model and the thermal information provided by the satellite developer. They are the most detailed design information to be used to construct the analytical solar radiation pressure and thermal radiation pressure models ever for QZSS satellites. We applied the pre-computed geometry tensor method for solar radiation pressure modeling and constructed a simple box-wing-hat thermal radiation pressure model. In particular, this thermal radiation pressure is the first model constructed with realistic temperature information. Based on the analytical model, we also proposed a hybrid model combined with the empirical approach. The accurate force models were implemented on a precise orbit determination tool called MADOCA, and orbit determination experiments were performed for QZS-1, 2, and 4. The results show that the proposed analytical model has better accuracy in orbit determination than the currently published orbit products obtained by empirical disturbance models.

**Keywords** Solar radiation pressure · Thermal re-radiation pressure · Precise orbit determination · QZSS

## Introduction

The centimeter-level precise orbit determination (POD) of navigation satellites is essential for the Global Navigation Satellite System (GNSS) to provide accurate positioning results to its users. The Japanese Quasi-Zenith Satellite System (QZSS) must also provide precise centimeter-level orbit information. The Japan Aerospace Exploration Agency (JAXA) has been developing MADOCA (Multi-GNSS Advanced Demonstration tool for Orbit and Clock Analysis) since 2011, and the recent developments have mainly focused on improving the QZSS POD (Kawate et al. 2023). A precise orbit determination analysis requires accurate disturbance force models that act on navigation satellites. In

particular, modeling non-gravitational forces, such as solar radiation pressure (SRP) and thermal re-radiation pressure (TRP), is a major issue in achieving centimeter-level accuracy.

Many early studies proposed non-gravitational models for GNSS satellites (Fliegel et al. 1992; Fliegel and Gallini 1996; Beutler et al. 1994; and Rodriguez-Solano et al. 2012). These models are mainly categorized into two approaches: empirical and analytical. Empirical approaches assume that the non-gravitational forces are expressed by a combination of polynomials and periodic functions, and the coefficients in the functions are estimated within the orbit determination process using many observation data. By contrast, analytical approaches calculate the SRP and TRP using a surface model and the thermal and optical properties of the satellites. Since a pure analytical model cannot reduce the modeling error, hybrid approaches have been proposed to compensate for this error by combining empirical models (Montenbruck et al. 2015, 2017). For GNSS precise orbit determination, empirical models are commonly employed within the International GNSS Service (IGS) analysis center because these empirical models can provide accurate orbit despite

✉ Satoshi Ikari  
ikari@space.t.u-tokyo.ac.jp

<sup>1</sup> Aeronautics and Astronautics, The University of Tokyo, Tokyo, Japan

<sup>2</sup> JAXA, Tsukuba, Japan

<sup>3</sup> Mitsubishi Electric Corporation, Kanagawa, Japan

<sup>4</sup> Chubu University, Aichi, Japan

their simple expressions (Beutler et al. 1994). However, some studies still use analytical approaches owing to their advantages over empirical models. For example, analytical approaches can provide an accurate force model and precise orbit ahead of the launch of the navigation satellites without a large amount of observation data. They can also help reveal systematic error in the empirical models and understand orbital dynamics. These knowledges may be useful in the design and consideration of next-generation navigation systems; therefore, this study uses an analytical approach to construct the SRP and TRP of QZSS satellites.

One of the most important analytical approaches is the ray-tracing, which is used to construct an accurate SRP model of the GLONASS satellite (Ziebart 2001). Based on the ray-tracing method, a University College London (UCL) research group applied the latest high-precision analytical radiation force models to the Galileo spacecraft, achieving centimeter-level POD with an analytical model (Bhattarai et al. 2022). For the QZSS system, the authors proposed a box-wing-hat model to emulate the L-band antenna installed on the QZS-1 satellite and constructed a pure analytical SRP model; however the orbit determination accuracy did not reached the centimeter-level (Ikari et al. 2014). Darugna et al. (2018) constructed a 3D model of the QZS-1 satellite from the papercraft information and applied the ray-tracing method to calculate the analytical SRP, taking a hybrid approach. Yuan et al. (2020) have constructed an analytical box-wing-hat model by using the satellite meta data published by the Japanese Cabinet Office and combined the analytical model with the hybrid approach. Both research groups achieved centimeter-level POD accuracy with the hybrid approach. However, the previous studies used limited satellite information and relied on compensation by the empirical model. In this study, we used a high-fidelity satellite surface model, optical properties, and thermal design information provided by the QZSS satellite manufacturer. They are the most detailed design information to be used to construct the analytical solar radiation pressure and thermal radiation pressure models ever for QZSS satellites. We constructed an accurate SRP and TRP model to improve the analytical force modeling of the QZSS satellites. In particular, this thermal radiation pressure is the first model, which is constructed realistic temperature information.

In 2022, the QZSS system had four inclined geosynchronous orbit (IGSO) satellites (QZS-1, 2, 4, and 1R) and one geostationary orbit (GEO) satellite (QZS-3). This study focuses on the three IGSO satellites: QZS-1, 2, and 4. The non-gravitational force modeling method is described in the next section. Subsequently, the constructed analytical force model was implemented into the MADOCA and evaluated the orbit determination accuracy was evaluated using the Satellite Laser Ranging (SLR) residual and overlap error.

## Non-gravitational force modeling

This section introduces our proposed force modeling method for QZSS satellites. For the SRP modeling, we proposed the pre-computed geometry tensor (PCGT) method. The method is based on the ray-tracing approach to obtain the self-shadowing effects and it reduces calculation costs by using pre-computed geometry tensor with shadow approximation. For the TRP modeling, we used the box-wing approximation approach to calculate the TRP of each surface. Both models are constructed with the most detailed information as satellite surface model, optical properties, and thermal design information provided by the QZSS satellite manufacturer.

### Fundamental equations of SRP and TRP

The SRP force generated by the  $j$  th surface  $a_{SRP_j}$  is derived as follows:

$$F_{SRP_j} = -\frac{P}{c} V_j(\mathbf{i}) A_j (\mathbf{i} \cdot \mathbf{n}_j) \left[ \mathbf{i} + C_{sj} \{2(\mathbf{i} \cdot \mathbf{n}_j) \mathbf{n}_j - \mathbf{i}\} + \frac{2}{3} C_{dj} \mathbf{n}_j \right] \quad (1)$$

$$P = P_{\odot} SF \left( \frac{1AU}{d_{\odot}} \right)^2$$

where  $A_j$ ,  $C_{sj}$ ,  $C_{dj}$ , and  $\mathbf{n}_j$  are the area, specular reflectance, diffuse reflectance, and unit normal vector, respectively, of the  $j$  th surface.  $V_j(\mathbf{i})$  is the binary visibility function of the  $j$  th surface.  $V_j(\mathbf{i}) = 1$  when the surface is illuminated, and  $V_j(\mathbf{i}) = 0$  when the surface is unilluminated.  $\mathbf{i}$  is the unit vector of the sun;  $c$  is the speed of light;  $P_{\odot}$  is the solar constant;  $d_{\odot}$  is the distance between the sun and the spacecraft, and  $SF$  is the shadow function, which expresses the eclipse effect.

The TRP force generated by the  $j$  th surface  $a_{TRP_j}$  is derived as follows (Milani et al. 1987):

$$F_{TRP_j} = -\frac{2}{3} \frac{1}{c} A_j \sigma \epsilon_j T_j^4 \mathbf{n}_j \quad (2)$$

where  $A_j$ ,  $\epsilon_j$ ,  $T_j$ , and  $\mathbf{n}_j$  are the area, emissivity, temperature, and normal direction of the  $j$  th surface, respectively;  $\sigma$  is the Stefan-Boltzmann constant; and  $c$  is the speed of light.

### Satellite information

To construct accurate analytical force models, satellite surfaces information, optical properties of the surfaces, thermal information or temperature information of the surfaces, attitude information, and satellite mass are required. Modeling accuracy is strongly related to the fidelity of this information. This subsection describes the satellite information we used in this study.

A high-fidelity satellite surface model is essential to accurately model SRP and calculate the self-shadow effect and multiple reflections on the surfaces. In this research, we used high-fidelity satellite surface models generated from the Computer Aided Design (CAD) data of QZSS satellites provided by the satellite manufacturer MELCO (Mitsubishi Electric Corporation). Figure 1 shows the CAD data of the satellite bodies of the QZS-1, 2, and 4 satellites. The structures of QZS-2 and 4 are the same, but structure of QZS-1 is slightly different around the Earth-side plane. Solar panels are not considered because they do not produce self-shadows on the body surface and vice versa in the QZSS attitude definition. In the Orbit Normal (ON) mode of QZS-1, the rods of the solar panels shadow on the positive and negative Y plane; however, this is ignored in this study. The SRP acting on the solar panels is simply modeled as a pressure acting on a flat surface.

The authors measured the optical properties of each outer surface, and some of the results were published as QZSS satellite metadata on the webpage of the Japanese Cabinet Office (Cabinet Office 2023). MELCO provided test pieces of the QZS-2 and 4 surface materials, and we measured the total reflectance and the specular coefficient of each material in the wavelength range of 250 nm to 2500 nm, which covers the sunlight spectrum. We used an Agilent Cary 5000 UV–Vis–NIR spectrophotometer and a Cary 7000 universal measurement spectrophotometer

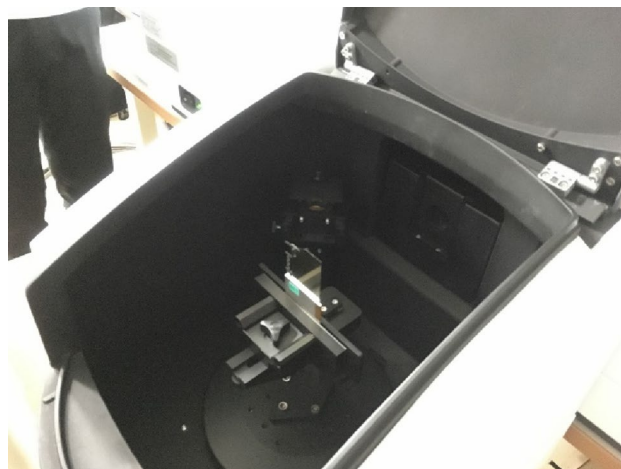
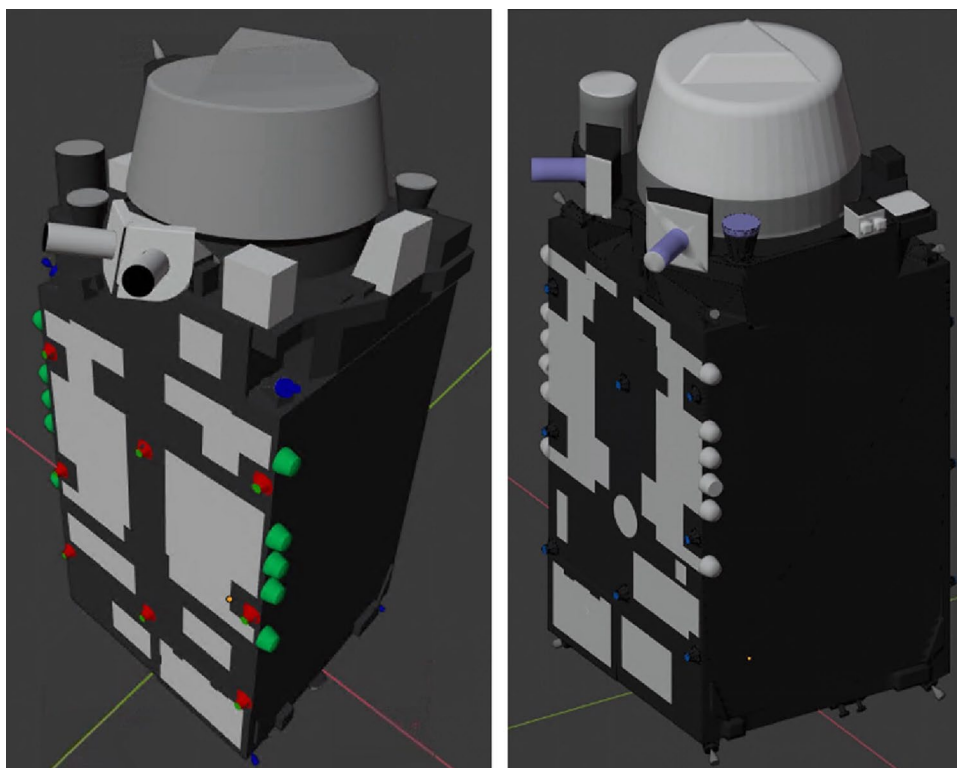


**Fig. 2** Optical property measurement. We used the Agilent Cary 5000 UV–Vis–NIR spectrophotometer and a Cary 7000 to measure the total reflectance and specular reflectance with wavelength dependency

(UMS) for the total reflectance and specular reflectance measurements, respectively (Fig. 2). We selected an incident angle of 45 degrees for specular reflectance measurements. To obtain the total reflectance and specular reflectance for sunlight, the measured reflectance spectrum was multiplied by the sunlight spectrum and integrated by wavelength. We measured three test pieces for each

**Fig. 1** CAD data of QZS-1 (left) and QZS-2 and 4 (right). The CAD data are provided by satellite manufacturer MELCO and used to construct high-fidelity solar radiation pressure models



material, and the average of the three measured reflectance values was used in this study. The total reflectance  $\nu$  and the specular coefficient  $C_s$  were converted to the absorption,  $\alpha$ ; diffuse reflectance,  $C_d$ ; and specularity,  $\mu$  with the following equations. In this research, we used  $C_s$  and  $C_d$  to calculate the SRP and  $\alpha$  to calculate the TRP. We used the satellite design data provided by MELCO and JAXA as the QZS-1's optical properties.

$$\alpha + C_s + C_d = 1 \tag{3}$$

$$\alpha = 1 - \nu \tag{4}$$

$$C_d = 1 - \alpha - C_s = \nu - C_s \tag{5}$$

$$\mu = \frac{C_s}{\nu} \tag{6}$$

The TRP calculations require the temperature and emissivity of each surface. As thermal information, MELCO provides a time series temperature history of representative satellite surfaces during an orbital period. The representative surfaces used to calculate the TRP were determined based on the box-wing-hat model of the QZSS satellites. The thermal environment of a spacecraft depends on the  $\beta$  angle, which varies by season. To evaluate the  $\beta$ -angle effect, four specific dates were chosen to generate the time-series history. The temperature of the surfaces was calculated from the numerical thermal model for accurate thermal analysis of

the satellites, including the orbit, attitude, and internal component power consumption. The numerical thermal model was calibrated using the thermal vacuum test results and the initial operation results after the satellite launch.

Satellite attitude, mass, and definition of body-fixed frame information are available on the Japanese Cabinet Office web page (Cabinet Office 2023). QZS-1 has two attitude modes: Yaw Steering (YS) and Orbit Normal (ON). QZS-2 and 4 only have the YS mode. In the YS attitude mode, the sun direction varies in the minus X half-circle area in the X–Z body plane. In the ON mode, all planes including the Y-plane, which is the heat-radiation plane, are illuminated by the sun.

### SRP modeling

Generally, to derive an accurate SRP, we need to consider the self-shadowing effect and multiple reflection effect, but their calculation cost is very high. Therefore, to reduce the cost, we applied the pre-computation method proposed by Ikari et al. (2017) and called it the pre-computed geometry tensor (PCGT) method (Fig. 3). In the PCGT method, the surfaces in the satellite model are divided into many polygons, and the binary visibility function of each polygon  $V_j(i)$  is derived by using ray-tracing calculations in the pre-computation phase. The visibility functions  $V_j(i)$  are approximated by the arbitrary approximation function  $\varphi_k(i_b)$ , and the pre-computed tensors  $T_{kb'}$ ,  $U_{s_{mkb'bb}}$ , and  $U_{d_{mkb'b}}$  are calculated for each material.  $T_{kb'}$ ,  $U_{s_{mkb'bb}}$ , and  $U_{d_{mkb'b}}$  are the incident light momentum effect, the specular reflection effect, and the diffuse reflection effect, respectively. In the

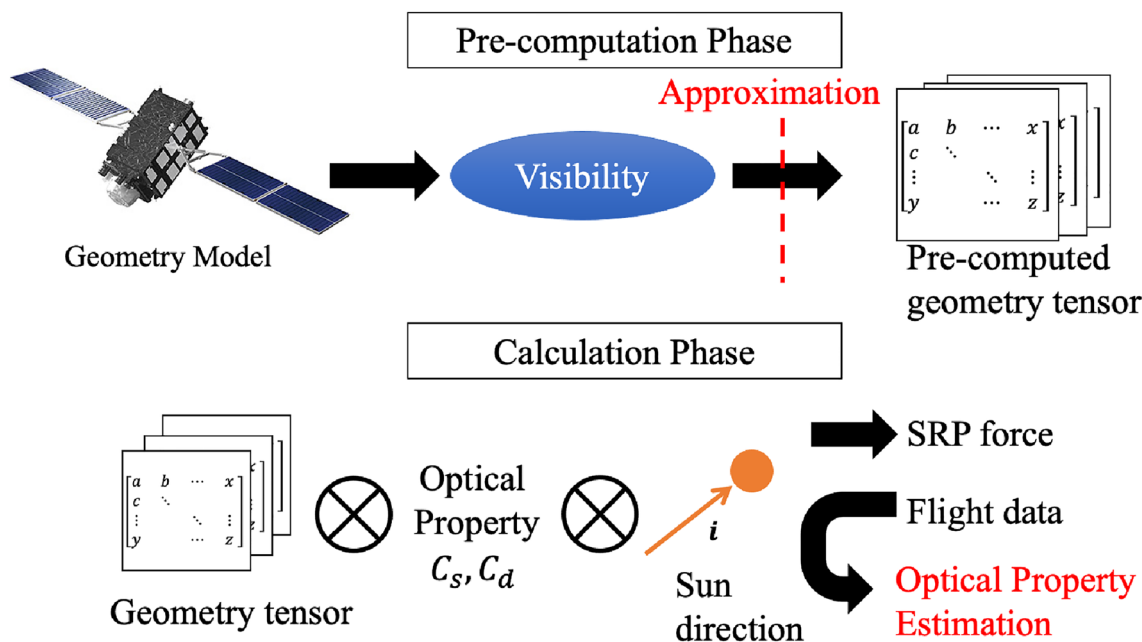


**Fig. 3** Overview of PCGT method. The pre-computed geometry tensors are calculated in the pre-computation phase with the ray-tracing method, and the tensors are used in the calculation phase with low computational cost

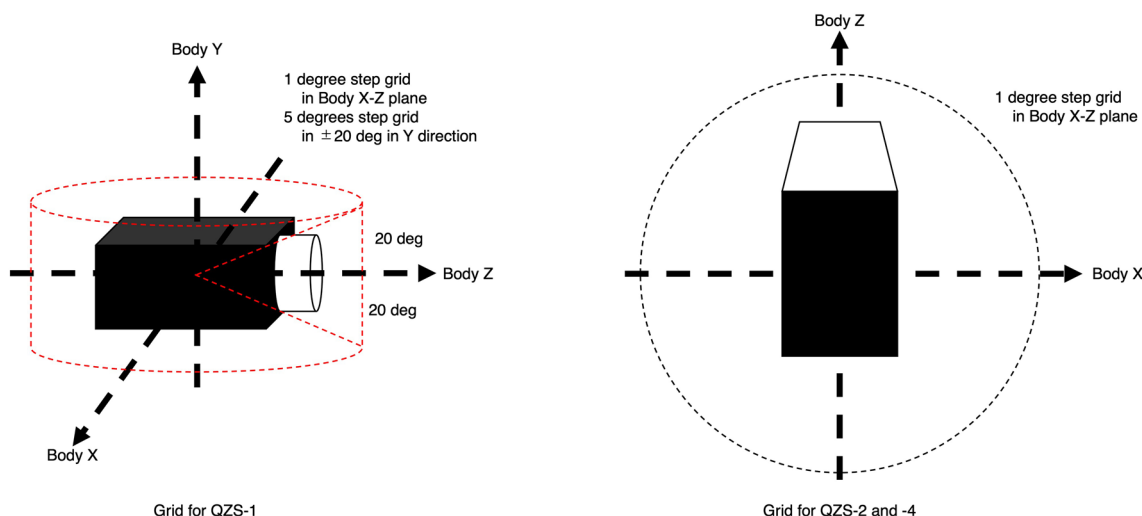


Fig. 4 Grid definition of the piecewise linear function. We used a three-dimensional grid for QZS-1 because it has the ON attitude mode

real-time phase, the SRP force  $F_{SRPb}$  is calculated using the tensors and optical properties  $C_{sm}$  and  $C_{dm}$  of the material  $m$ .

Details of the TRP models are described in the following subsections.

$$F_{SRPb} = -\frac{P_{\odot}}{c} \left\{ T_{kb'} i_b + i_b \sum_{m=1}^M (C_{sm} U_{smkb'bb}) + \frac{2}{3} \sum_{m=1}^M (C_{dm} U_{dmb'bb}) \right\} \varphi_k(i_b) i_{b'} \tag{7}$$

We chose a piecewise linear function as the approximation function  $\varphi_k(i_b)$ . The grid of the piecewise linear function is shown in Fig. 4. QZS-1’s SRP model consists of nine materials, and QZS-2 and 4 SRP models consist of nine materials. The  $C_{sm}$  and  $C_{dm}$  can be easily changed without recalculating the visibility functions and can be estimated together with the orbit determination process. However, this study does not estimate the optical parameters, which will be the subject of future work.

**TRP modeling**

We constructed the TRP model for QZSS satellites based on a simple box-wing-hat shape constructed using solar panels, body surfaces, and L-band antenna covers. We first calculated the TRP model using (2) with the manufacturer-provided temperature and emissivity of each satellite surface to construct the TRP model. However, the calculated TRP was not used for the POD calculation because it was difficult to directly estimate the surface temperature during the POD process. We only used the input thermal energy and some parameters to model the TRP force with respect to the sunlight incident angle of each surface. We estimated the modeling parameters from the calculated TRP; therefore, our model does not require the surface temperature itself.

**Solar panels**

The thermal information indicates that the temperatures of the solar panels are stable during the orbital period for all the QZSS satellites. The temperatures of the front and back sides of the solar panels were 40 degrees and 28 degrees, respectively, for QZS-1 in both YS and ON modes; and 70 degrees and 38 degrees, respectively, for QZS-2 and 4. We modeled the TRP of the solar panels as shown in the following equation to consider the effect of the incoming solar power,

$$F_{TRP_{SAP}} = -P_{\odot} \left( \frac{1AU}{d_{s\odot}} \right)^2 C_{TRP_{SAP}} n_{sap} \tag{8}$$

where the  $C_{TRP_{SAP}}$  was derived from the temperature information as  $8.4 \times 10^{-6}$  N for QZS-1 and  $1.5 \times 10^{-5}$  N for QZS-2 and 4. The solar panel area of QZS-1 is larger than that of QZS-2 and 4, but the TRP of QZS-1 is smaller than that of QZS-2 and 4 because the temperatures of QZS-2 and 4 are higher than that of QZS-1.

**Body X-plane**

The body X-planes of the QZSS satellites are covered by black multi-layer insulation (MLI), which isolates the heat



flux between the outer surface and inside of the satellite; most of the absorbed solar energy is reradiated as a diffuse emission. Based on these characteristics, we modeled the TRP of the X-plane as follows:

$$F_{TRP_{MLI}} = -\frac{2}{3} \frac{P_{\odot}}{c} \left(\frac{1AU}{d_{s\odot}}\right)^2 A_{MLI} \alpha_{MLI} \cos \theta \mathbf{n}_{MLI} \begin{cases} c_{MLI} \cos \theta > 0 \\ 0 \cos \theta \leq 0 \end{cases} \tag{9}$$

where  $\theta$  is the angle between the normal vector of the plane and the sun direction vector, and  $0 < c_{MLI} \leq 1$  is the correction factor for expressing the imperfect isolation of the MLI.

Using (2) and the provided temperature history, we independently calculated the TRP of the X-plane and determined that the behavior is similar to that of (9). We derived the  $c_{MLI}$  to fit the TRP calculated by (2); this value was 0.99 for QZS-1, 2, and 4, including QZS-1's ON mode. This means that most of the heat energy is re-emitted, but 1% of the energy is absorbed into the satellite's internal body. For QZS-1's ON mode, Fig. 5 shows the magnitude of calculated TRP

force using (2) ( $F_{px}$  and  $F_{mx}$ ) and the estimated magnitude of TRP force using (9) ( $Fest_{px}$  and  $Fest_{mx}$ ).  $\dot{m}_x$  and  $\dot{p}_x$  mean force acting on the minus and plus X-plane, respectively.  $\theta_x$  is the angle between the body X direction and the sun direction vector. The estimation model accurately expresses the calculated TRP forces without the temperature information of the surfaces. The maximum TRP value reaches 2.5 uN, which is 10% of the maximum value of the SRP force. This means the TRP effect is large for QZSS satellites to be considered to make high-fidelity analytical disturbance models.

### Body Y-plane

The body Y-planes of the QZSS satellites have several radiation panels, and the other regions are covered by the black MLI. Both the plus and minus Y-planes are not illuminated by the sun in the YS attitude mode, and the TRP generated by the planes is very small. We modeled a small constant of  $7.6 \times 10^{-7}$  N on the Y-axis using the provided temperature information and (2). In the ON mode of QZS-1, the Y-plane is illuminated by the sun, and the MLI temperature of the illuminated Y-plane increases. However, the temperatures of the radiation panels of both the plus and minus Y-plane are still stable, and the heat radiation is canceled by the plus and minus planes. Therefore, we only need to consider the TRP using the illuminated MLI on the Y-plane. Equation (9) can be used to calculate the TRP of the illuminated MLI;  $c_{MLI}$  of the minus Y-plane was estimated to be 1.04, indicating unknown additional heat radiation on the MLI. The cause of the additional radiation is unclear, but it may be due to the mismodeling of the thermal model, including the error in the thermal properties of the surfaces.

### Body Z-plane

The plus Z-plane has many antennas and components and generates complex thermal radiation. To simplify the model, only a flat plane and the L-band antenna were assumed. Details of the antenna cover are described in the following subsections. The minus Z-plane has a black MLI surface and an apogee kick motor structure, and the provided thermal information includes that of both the MLI and the motor.

The TRP modeling is not as simple for mixed-material surfaces as for pure MLI surfaces. We modeled the TRP of the mixed-material surfaces using the following equation,

$$F_{TRP_{mixed}} = -\frac{2}{3} \frac{P_{\odot}}{c} \left(\frac{1AU}{d_{s\odot}}\right)^2 A_{mixed} \alpha_{mixed} |\cos \theta_{mixed}| \mathbf{n}_{mixed} \begin{cases} (c_1 + o) \cos \theta_{mixed} > 0 \\ (c_2 + o) \cos \theta_{mixed} \leq 0 \end{cases} \tag{10}$$

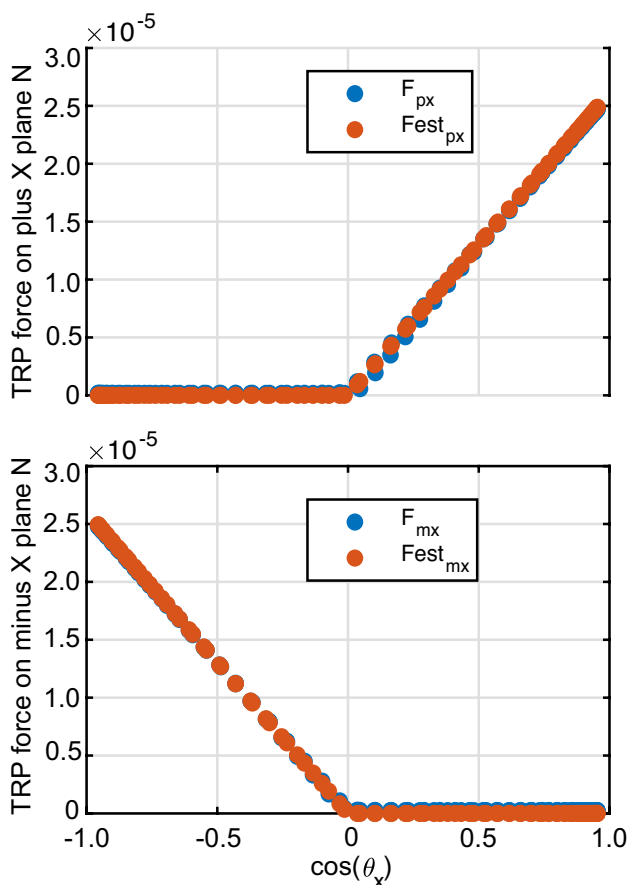
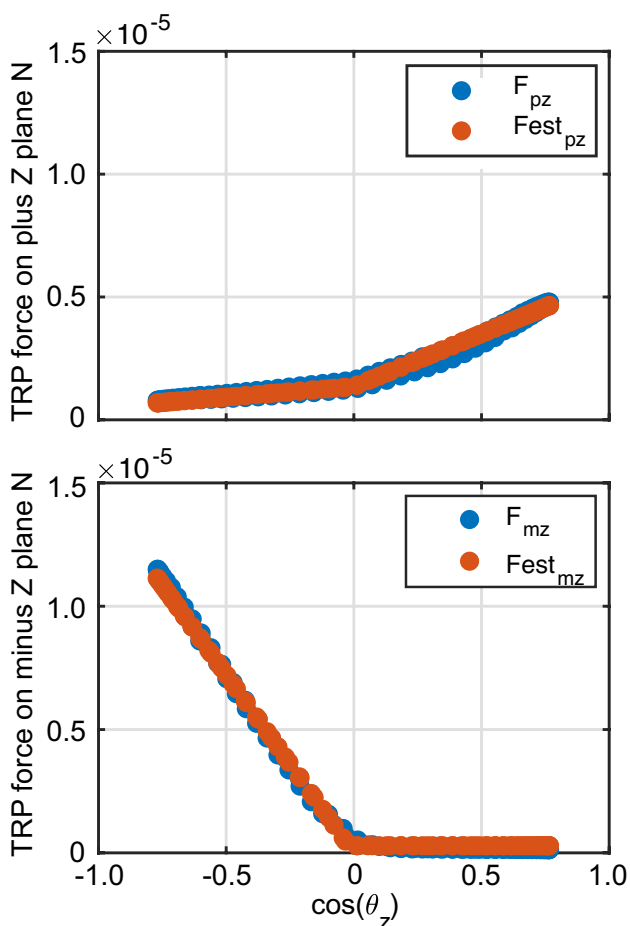


Fig. 5 TRP of X-plane when  $\beta = 17$  degrees. The top shows the plus X-plane, and the bottom shows the minus X-plane. Calculated and estimated TRPs are shown to indicate the correctness of the TRP model

**Table 1** TRP model parameters for Z-plane. The parameters are estimated from the provided thermal information for each satellite. We need to change the value depending on the attitude mode of QZS-1

	QZS-1, 2, and 4 YS mode		QZS-1 ON mode	
	PZ	MZ	PZ	MZ
$o$	Q2, 4: 0.115 Q1: 0.08	0	0.1	0
$c_1$	Q2, 4: 0.55 Q1: 0.48	Q2, 4: 0.98 Q1: 0.9	0.6	0.97
$c_2$	Q2, 4: 0.165 Q1: 0.2	0.02	0.2	0.02



**Fig. 6** TRP of Z-plane in YS mode. The top shows the plus Z-plane, and the bottom shows the minus Z-plane. Calculated and estimated TRPs are shown to indicate the correctness of the TRP model

In the case of Z-plane, we used  $\theta_{mixed}$  as  $\theta_z$ , and  $\mathbf{n}_{mixed}$  as  $\mathbf{n}_z$ . The values of  $A_{mixed}$  and  $\alpha_{mixed}$  were sourced from the QZS-1 satellite metadata (Cabinet Office 2023). We used  $\alpha_{mixed}$  of the largest area material. The base equation is similar to that

**Table 2** TRP model parameters of L band antenna cover for QZS-1, 2, and 4. The parameters are estimated from the provided thermal information in the YS mode

	Truncated Cone part	Cylinder part
$o$	0.22	0.9
$c_1$	0.2	-0.1
$c_2$	0.38	2.0

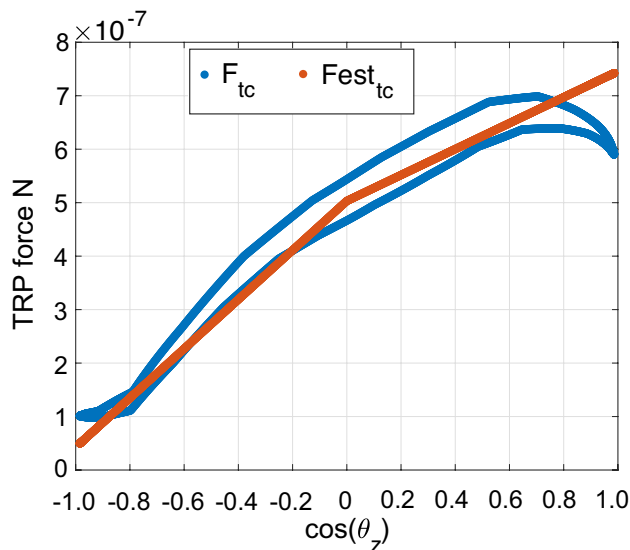


**Fig. 7** TRP of truncated-cone surface of the L-band antenna in YS mode. Calculated and estimated TRPs are shown to indicate the correctness of the TRP model

of pure MLI surfaces, but additionally includes the heat-radiation offset  $o$  and the heat residual factor  $c_2$  when the surface is on the shadow side. The parameters were estimated using the thermal information provided. The estimated parameters are listed in Table 1. The magnitude of TRP calculated from the thermal information ( $F_{pz}$  and  $F_{mz}$ ) and magnitude of estimated TRP using (10) and parameters listed in Table 1 ( $Fest_{pz}$  and  $Fest_{mz}$ ) are shown in Fig. 6, which shows that the estimation error is sufficiently small. The  $\hat{m}_z$  and  $\hat{p}_z$  mean force acting on the minus and plus Z-plane, respectively.  $\theta_z$  is the angle between the body Z direction and the sun direction vector.

**L-band antenna**

The side surface of the L-band antenna cover is divided into the cylinder side and the truncated-cone side. The cover material consists of single-layer insulation (SLI), which reflects solar light but passes through the radio wave from the L-band antenna. The insulation performance of the SLI is worse than that of MLI, and other heat sources exist

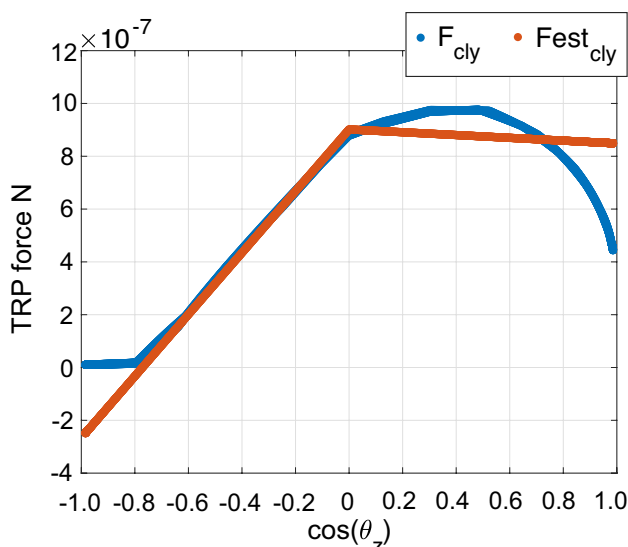


**Fig. 8** TRP of cylinder surface of the L-band antenna in YS mode. Calculated and estimated TRPs are shown to indicate the correctness of the TRP model

**Table 3** TRP model parameters of the truncated-cone part of the L-band antenna. The parameters are estimated from the provided thermal information of QZS-1 in the ON mode

	Sun on +X	Sun on -X
$o$	0.15	0.17
$c_1$	0.1	-0.05
$c_2$	0.35	0.2

**Table 4** TRP model parameters of the cylinder part of the L-band antenna. The parameters are estimated from the provided thermal information of QZS-1 in the ON mode

	Sun on +X	Sun on -X
$o$	0.05	0.23
$c_1$	0.2	0.2
$c_2$	0	0.75

around the cover. It is difficult to use a simple TRP model for MLI. We modeled the TRP of the SLI of the L-band antenna cover in the same manner as the mixed material, as in (10) in the YS mode for QZS-1, 2, and 4. Table 2 summarizes the estimated parameters from the TRP calculated from the thermal information in the YS mode for QZS-1, 2, and 4. Figures 7 and 8 show the calculated TRP ( $F_{tc}$  and  $F_{cly}$ ) and the estimated TRP using (10) and the parameters given in Table 2 ( $Fest_{tc}$  and  $Fest_{cly}$ ). We can see that the calculated TRPs have hysteresis depending on the moving direction of the sun angle, and a large error arises when the sun is on the plus Z-axis. However, we ignored these errors because they are only  $4 \times 10^{-7}$  N in maximum and thus sufficiently small. The cause of the hysteresis was unclear, but we consider that the heat-keeping effect of the L-band

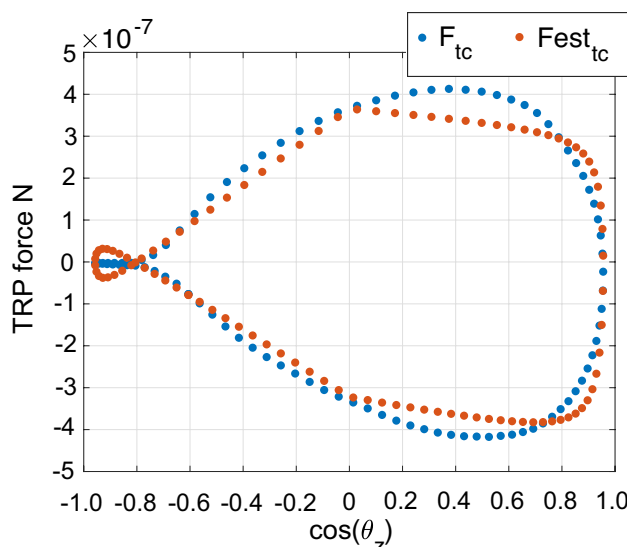


**Fig. 9** TRP of truncated-cone surface of the L-band antenna for QZS-1's ON mode. Calculated and estimated TRPs are shown to indicate the correctness of the TRP model

antenna may be the cause. The direction of the TRP output is  $[1, 0, 0]$  for the cylinder side and  $[0.98, 0, 0.18]$  for the truncated cone side on the body frame. The direction of the truncated cone is defined from the shape of the truncated cone described in the QZS-1 satellite metadata (Cabinet Office 2023).

In the ON mode of QZS-1, the hysteresis was more significant than that of the YS mode for both the cylinder and truncated-cone parts. The equation is basically the same as (10), but the parameters must be changed according to the sun direction to emulate the hysteresis behavior. Tables 3 and 4 list the estimated parameters from the thermal information provided in the ON mode. The parameters are changed by the sign of the X-component of the sun direction on the body frame. The direction of the TRP output of the truncated cone  $n_{tc}$  and that of the cylinder  $n_{cly}$  were calculated using the following equations.

$$n_{tc} = \frac{1}{\sqrt{(0.98u_x)^2 + (0.98u_y)^2 + 0.18^2}} \begin{bmatrix} 0.98u_x \\ 0.98u_y \\ 0.18 \end{bmatrix} \quad (11)$$

$$n_{cly} = \frac{1}{\sqrt{u_x^2 + u_y^2}} \begin{bmatrix} u_x \\ u_y \\ 0 \end{bmatrix} \quad (12)$$

where  $u_x$  and  $u_y$  are the X- and Y-components, respectively, of the sun vector in the body frame. We used the direction vectors  $n_{tc}$  and  $n_{cly}$  as the  $n_{mixed}$  in (10).



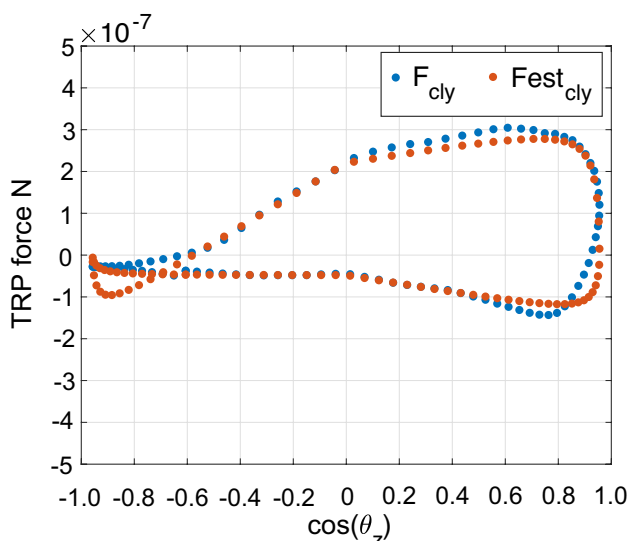


**Fig. 10** TRP of cylinder surface of the L-band antenna for QZS-1’s ON mode. Calculated and estimated TRPs are shown to indicate the correctness of the TRP model

Figures 9 and 10 show the calculated TRP ( $F_{tc}$  and  $F_{cly}$ ) and the estimated TRP using (10) and the parameters given in Tables 3 and 4 ( $Fest_{tc}$  and  $Fest_{cly}$ ). The TRP estimated using (10) and the parameters well approximate the calculated TRP by the given thermal data. The maximum error is  $2.7 \times 10^{-7}$  N and is sufficiently small.

**Limitations of the analytical models**

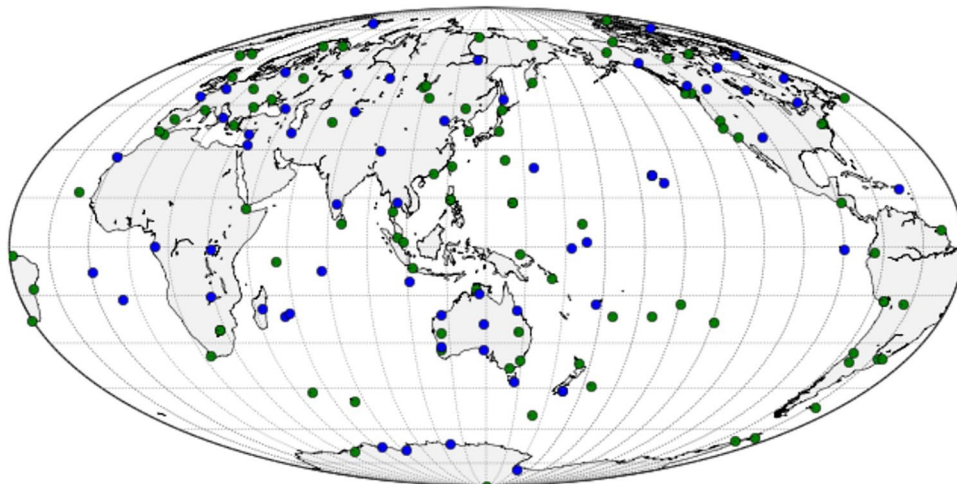
The constructed analytical SRP and TRP models for QZSS satellites have modeling errors because the provided satellite information provided does not perfectly represent

on-orbit satellites. In particular, the MLIs are not perfectly mounted on the surfaces, as in the CAD model and have unmodeled wrinkles. The optical properties also exhibit measurement and modeling errors, ignoring the complex reflection behavior. These properties were degraded by the aging effect on the orbit. Even if the provided satellite information is accurate, several approximations exist in the proposed models. The PCGT method ignores the multiple reflection effect, and the TRP model ignores the complex shapes of plus and minus Z-planes. We cannot completely remove these errors from the analytical models. Hence, we need to compensate for these errors using the hybrid approach. This study combines the proposed analytical and empirical models to make a hybrid model. The details of the combined empirical model is described in the next section.

**POD experiment and results**

This chapter reports the POD performance results when the proposed SRP and TRP models are applied as a priori non-gravitational force models. These models were implemented on three QZS satellites (QZS-1, 2, and 4) in an inclined geostationary orbit (IGSO). For the evaluation period, April 2021–March 2022 was selected as the most recent period during which these three satellites were active. This period covers almost two complete cycles of the beta angles of the satellites. A special version of MADOCA v1.0.1 POD software (Kawate et al. 2023), which makes the PCGT SRP and TRP models described in the previous chapters available as a priori non-gravitational force models, was used for the evaluation. The parameters used in the models, the satellite CAD model, optical characteristics, and TRP correction factor based on the satellite surface temperature, were set to the

**Fig. 11** Map of reference stations used in the experiments. We used globally distributed IGS multi-GNSS and legacy IGS stations



values presented in the previous section. The satellite masses used to convert the non-gravitational force calculated by the proposed model into the corresponding acceleration were applied for each evaluation date from the time series data available on the QZSS website (Cabinet Office 2023).

Dual-frequency GPS and QZSS observations provided by a global network of IGS multi-GNSS stations (Montenbruck et al. 2017) and legacy IGS stations were used to perform a combined POD of the QZSS and GPS. The observation stations were selected mainly from the Asia-Oceania region to ensure a sufficient number of QZSS observations and tracking geometry. Figure 11 shows the global distribution of the IGS multi-GNSS and legacy IGS stations used for this evaluation. The blue points in Fig. 11 show the fiducial stations used to align the GPS and QZSS orbits with the IGB14 reference frame (Rebischung 2020), and the green points represent stations whose coordinates were estimated with free constraints.

In the POD processing, the PCGT SRP and TRP models were applied as a priori models for the non-gravitational acceleration of QZSS satellites, and five empirical ECOM

parameters (Springer et al. 1999) were estimated to compensate for the acceleration obtained by these models. To confirm the contribution of these a priori models, we also independently ran a case in which only seven empirical ECOM2 parameters (Arnold et al. 2015) were estimated without using the a priori model. The attitude of the QZS-1 shifts from the YS mode to the ON mode when the beta angle is below 20 degrees, where the solar panel axis is maintained perpendicular to the orbital plane (Montenbruck et al. 2015). Since the ECOM/ECOM2 model assumes that the GNSS attitude is in the YS mode, the D, B, and Y axes defined in the ECOM/ECOM2 model may not be directly applicable during the period when the QZS-1 attitude is in ON mode. Therefore, the modified DBY coordinate frame ( $e_d, e_b, e_y$ ) shown in the following equation was used during the ON mode:

$$e_d = e_s, \quad e_b = \frac{e_p \times e_s}{|e_p \times e_s|}, \quad e_y = e_d \times e_b \quad (13)$$

**Table 5** Processing summary of MADOCA. The following settings are used in our precise orbit determination experiments

Parameter	Value
GNSS	GPS and QZSS
Observations	Undifferenced L1-L2 ionosphere-free code and phase (GPS: L1C/A and L2P(Y), QZSS: L1C/A and L2C)
Arc length	30 h (3 + 24 + 3)
Data interval	5 min
Stations	151 stations on average (68 of which track QZSS)
Station Coordinate	Fiducial Stations: tightly constrained to ITRF2014(IGb14) Other stations: loosely constrained to single-point solution
Satellite PCO and PCVs	igs14.atx (Rebischung and Schmid 2016)
Troposphere	ZTD and Gradient: estimated as piece wise constant every 2 h ZHD: Saastamoinen model (Saastamoinen 1972) and global pressure–temperature (GPT) (Böhm et al. 2007) Mapping Function: Global mapping function (Boehm et al. 2006)
a priori EOPs	IERS Bulletin A
Sub-daily EOP corrections	Applied according to IERS Conventions 2010
Geopotential	EGM2008 (Pavlis et al. 2012) up to degree and order of 12. Tidal variations of solid Earth tides, ocean tides, solid Earth pole tide, and oceanic pole tide (Petit and Luzum 2010) are considered
Third body	Sun, Moon, Venus, and Jupiter (point of mass) Ephemeris: JPL DE421 (Folkner et al. 2009)
Solar Radiation Pressure and Thermal Radiation Pressure	GPS: nine ECOM parameters which are constrained to a priori values ( $\sigma=0.3 \text{ nm/s}^2$ ) QZSS: (1) five ECOM parameters + proposed a priori PCGT SRP model and TRP model proposed in the previous chapter, (2) Seven ECOM parameters without a priori model Earth albedo and antennal thrust are not applied for GPS and QZSS
Empirical accelerations	Piecewise constant every 12 h in radial, along-track, and cross-track directions for GPS and QZSS
Relativistic effects	Applied according to IERS Conventions 2010
Parameter estimates	Initial state vector for each satellite, station coordinates, troposphere ZTDs and gradients, satellite, and receiver clocks, EOPs, ECOM parameters, empirical accelerations, inter system biases, and phase ambiguities (IAR)

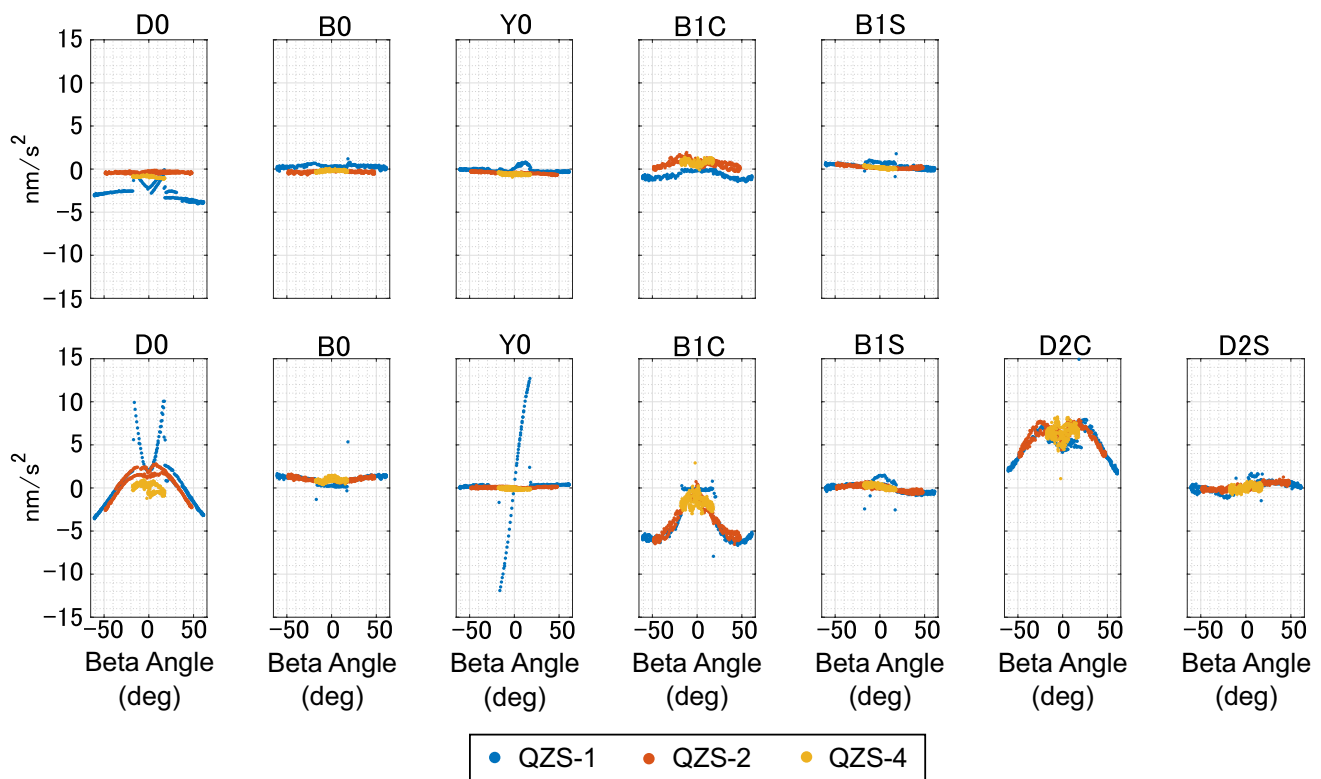


**Fig. 12** Estimated ECOM parameters. The horizontal axis shows the beta angle. The five ECOM parameters were estimated with a priori PCGT SRP and TRP model (top), and seven ECOM2 parameters were estimated without a priori model (bottom)

where  $e_s$  in (13) is the unit vector from the satellite to the sun (positive toward the sun), and  $e_p$  is the unit vector in the angular momentum direction of the orbit. It should be noted that  $e_y$  in ON mode does not coincide with the direction of the rotation axis of the satellite solar panel. This specific coordinate definition for the ON mode is the same as the terminator coordinate system of the ECOM-TB model (Prange 2020), and it improves the POD accuracy in the ON mode. A summary of the model and analysis strategy for the combined POD of QZSS and GPS is presented in Table 5.

### SRP parameter estimation

The ECOM parameters estimated with and without the a priori model are shown in Fig. 12. The average D0 value for each satellite was subtracted from the plot of D0 estimations without the a priori model. Among the seven ECOM2 parameters without the a priori model, D0, B1C, and D2C showed clear variations depending on the beta angle. The peak-to-peak values of variation for each parameter (D0, Y0, B1C, and D2C) exceed  $5 \text{ nm/s}^2$ . When the beta angle of QZS-1 is less than 18 degrees, there is a parabolic variation in D0, with a peak-to-peak value

approaching approximately  $10 \text{ nm/s}^2$ , and a linear variation in Y0 exceeding  $\pm 10 \text{ nm/s}^2$ .

On the other hand, the variations in all five ECOM parameters estimated using the proposed SRP and TRP models as a priori non-gravitational force models are less than  $2 \text{ nm/s}^2$ , except for the D0 estimate for QZS-1. It should be noted that the variation in the D0 estimate for QZS-1 is also dramatically improved compared to the case without the a priori model. In the PCGT SRP and TRP models, only pre-launch measurements and the calibration value obtained during the initial on-orbit operation were used, except for the satellite mass. In addition, no fine-tuning modification of the model parameters was performed to minimize the value of the estimated ECOM parameters. The results provided here indicate that the accuracy of the analytical non-gravitational acceleration model constructed with only such pre-defined information for QZS-2 and 4 is better than  $2 \text{ nm/s}^2$ , and  $5 \text{ nm/s}^2$  for QZS-1.

For QZS-2 and 4, we believe that the  $1\text{--}2 \text{ nm/s}^2$  modeling error is caused by the accumulation of modeling simplifications. The proposed TRP model has a  $0.2 \text{ nm/s}^2$  error in the TRP modeling, as shown in Figs. 7 and 8. The optical property errors and satellite mass estimation errors can also produce a similar magnitude of acceleration errors. We

must combine an empirical parameter estimation method with analytical disturbance models to compensate for these modeling errors.

The bias observed in the D0 estimates of the PCGT SRP and TRP models for QZS-1 is considered because of errors in the optical properties and satellite mass estimation. For example, to explain the  $3 \text{ nm/s}^2$  bias value, a 0.03 measurement error is needed in the total reflectance of the solar cells or a 40 kg error is needed in the QZS-1 mass estimation. We believe that the leading cause of the bias error is the optical property error because the 40 kg mass estimation error is too large, and the on-orbit aging effect may cause optical property error over ten years of operation. In the D0 estimates of QZS-1, two lines with the same positive beta angle were found; the gap between the two estimated values was  $1 \text{ nm/s}^2$ . This was caused by the mass update after the sun acquisition mode (SAM) operation from 20 to 26 August 2021, as mentioned in the history information of the QZS-1 operation (Cabinet Office 2023). During the SAM operation, the satellite mass decreased by 17 kg. This mass change is significantly larger than the approximately 5 kg change that occurred during the nominal thrusting operation. Therefore, there is a possibility that the published mass information for QZS-1 during the SAM operation is incorrect. To explain the  $1 \text{ nm/s}^2$  jump up in the D0 estimate, a mass error of 15 kg is required. More detailed operation information is required to clarify this issue.

We have also to consider the effect of antenna thrust, earth albedo, and earth infrared radiation pressure. The magnitude of antenna thrust generated by the QZSS satellites is estimated as  $0.3 \text{ nm/s}^2$  for QZS-1 and  $0.7 \text{ nm/s}^2$  for QZS-2 and 4. It is expected that we may improve the analytical disturbance by adding the antenna thrust to decrease the estimated ECOM parameters in Fig. 12. The earth albedo and infrared radiation pressure acting on the QZSS satellites is relatively smaller than other GNSS satellites because the altitude of IGSO is higher than them. Evaluation of these effects will be our future work.

## POD performance

The POD performance using the proposed SRP and TRP models of QZSS was evaluated based on orbit overlaps, which is the consistency between adjacent orbital arcs and the residuals of the satellite laser ranging (SLR) measurements.

## Orbit overlap

The QZSS orbit generated in this experiment has a 30-h orbital arc with a three-hour overlap period before and after and a 24-h period beginning at midnight. Therefore, an

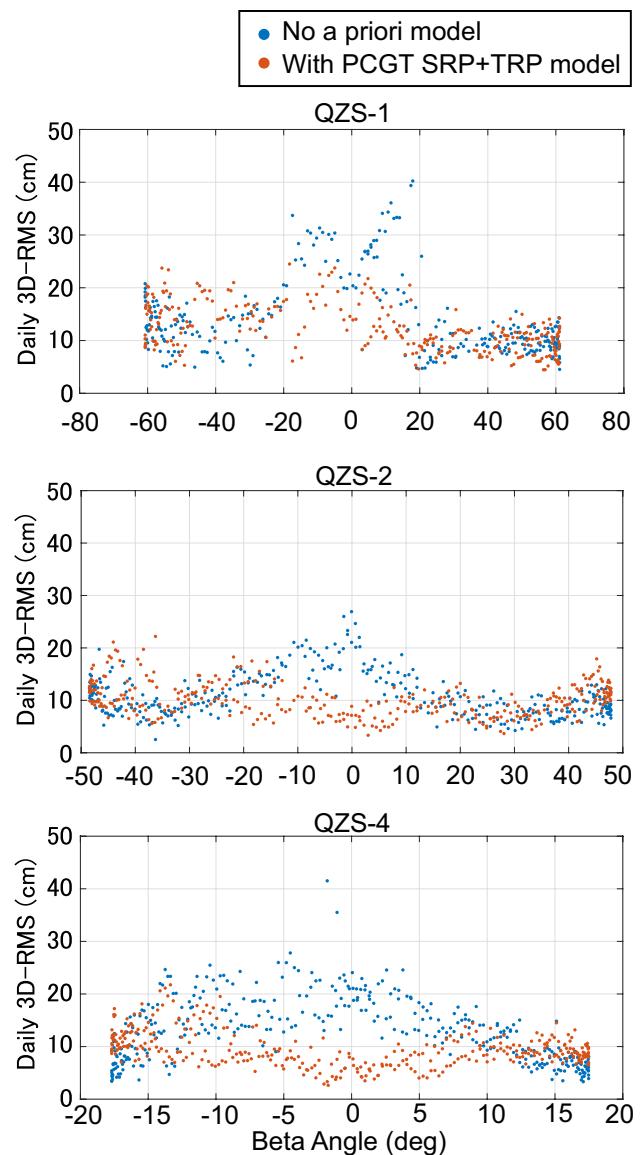


**Fig. 13** Orbit overlap daily 3D-RMS of QZSS satellites using different force models. The horizontal axis shows the beta angle. The proposed model especially improves the 3D RMS accuracy in low beta angles

overlap period of 6 h (21:00–03:00) per pair was obtained between adjacent orbital arcs.

Figure 13 shows the daily 3D-RMS values of the orbit overlap of each QZSS satellite with and without the proposed SRP and TRP models, with the beta angle on the horizontal axis. The daily 3D-RMS represents the RMS value of the difference between the satellite positions of adjacent orbital arcs over a daily overlap period of 6 h. A common feature of all QZS-1, 2, and 4 satellites is that the daily 3D-RMS of the orbit overlap with the proposed a priori model is smaller than that without the model during periods

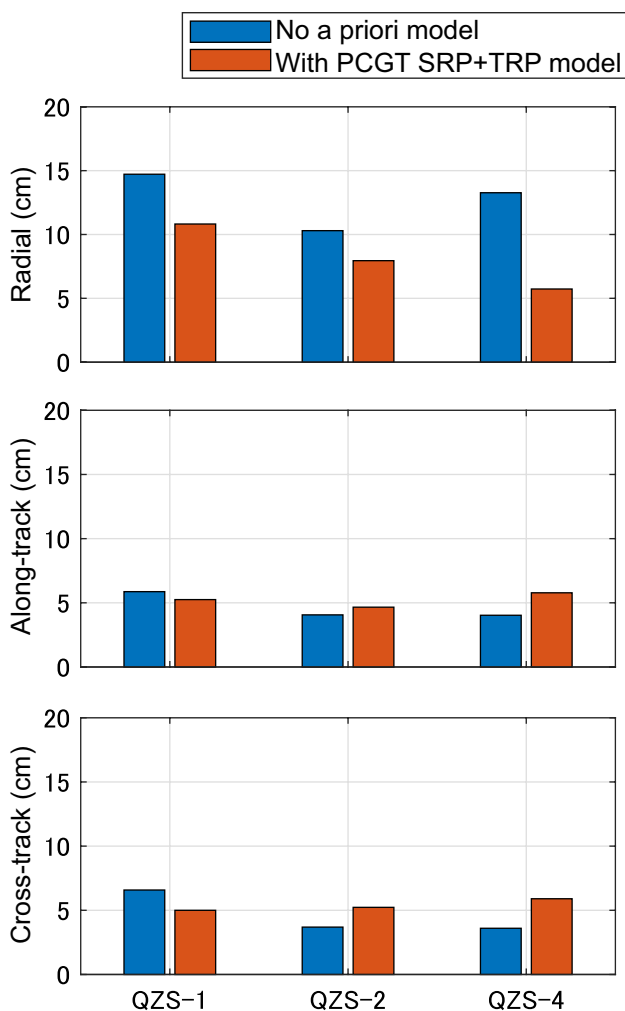


**Fig. 14** Orbit overlap RMS of QZSS satellites using different force models. The RMSs are calculated with the over one-year precise orbit determination results. The proposed model improves radial error

when the beta angle is smaller than 20 degrees. During this period, QZS-1 is in the ON mode, while QZS-2 and 4 are still in the YS mode. Therefore, the proposed SRP and TRP model is expected to improve the consistency of each orbit solution during the ON mode of the IGSO satellites and during the YS mode when the beta angle is relatively small.

To confirm the improvement of the orbit solution in more detail, Fig. 14 shows the RMS values of the overlap error over one year of the evaluation period for each component of the orbital radial, along-track, and cross-track directions. For QZS-1, 2, and 4 satellites, the RMS values of the proposed a priori model in the radial component are 10.8, 8.0, and 5.7 cm, respectively, which are 26.5, 22.6, and 56.8% better, respectively, than those of the seven ECOM2 parameters without a priori model. This indicates that the proposed SRP and TRP models can represent non-gravitational acceleration

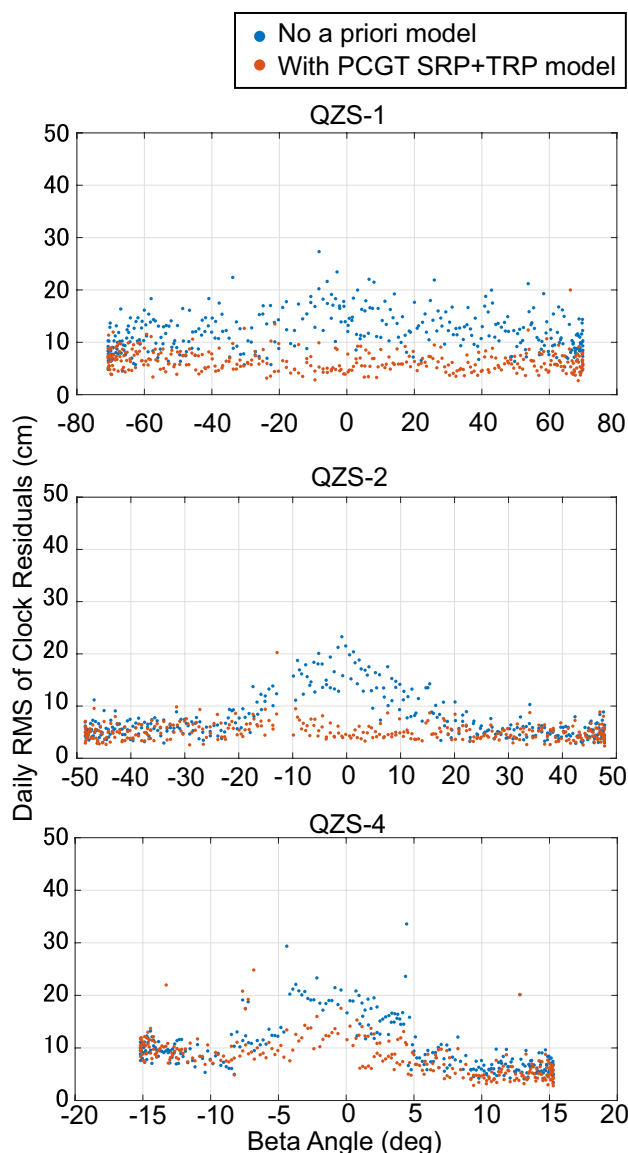


**Fig. 15** Linear Clock Fit Residuals of QZSS satellites using different force models. The horizontal axis shows the beta angle. Our proposed model provides better clock accuracy than the no a priori model for all satellites

more accurately than the existing ECOM2 model. However, the RMS values in the along-track and cross-track directions were slightly worse when the a priori model was used in the case of QZS-2 and 4. Further investigation is required to clarify this point.

**Linear clock fit residuals**

Assuming the characteristics of the highly stable GNSS satellites clock, the residuals of the estimated clock offsets



during an approximately 1-day period fitted with a linear function provide an indicator for evaluating the quality of the clock offset estimates. The linear clock fit residuals are also helpful in evaluating the accuracy of the orbit solutions since radial orbit errors are mapped to the estimated clock offset parameters (Montenbruck et al. 2015). Figure 15 shows the daily RMS values of the linear clock fit residuals. The residuals of QZS-2 clearly confirm the effect of the a priori model in the periods when the beta angle is less than 20 degrees; for the no a priori model, the daily RMS of the residuals increases as the absolute value of the beta angle decreases and exceed 20 cm when the beta angle is near zero degrees. On the other hand, with the proposed a priori model, the daily RMS of the residuals is less than 10 cm for all beta angles. In QZS-4, the beta angle is less than 20 degrees throughout the year, and the daily RMS of the residuals is smaller in all periods by applying the a priori model. While the clock residuals of QZS-1 do not clearly show the effect of the a priori model, the a priori model tends to reduce the overall residuals, including the period when the attitude mode of QZS-1 shifts to orbit normal mode with a beta angle of 20 degrees or less.

### SLR residuals

SLR measurements collected by the International Laser Ranging Service (ILRS; Pearlman et al. 2002) were used to assess the accuracy of the QZSS orbit. Seven stations located in the Asia-Oceania region, BEIL, CHAL, JFNL, KUN2, SHA2, STL3, and YARL, track QZSS satellites regularly. The station coordinates were fixed at the SLRF2014 (Pearlman et al. 2019), and outliers exceeding 0.5 m were rejected. The offset of the laser retroreflector array (LRA) with respect to the satellite center of mass was calculated based on the mass of each QZSS satellite as of October 1, 2021, the midpoint date of the evaluation period.

The SLR residuals of the QZSS satellite orbit estimated with and without the a priori model are shown in Fig. 16 as functions of the beta angle. In addition to the orbits with and without the a priori model, the JAXA final products provided by MGEX (Montenbruck et al. 2017) were also evaluated and added to the figure. The JAXA final products were generated by the MADOCA, and most of the algorithms are same as the other two models except for the disturbance modeling. Therefore, we can evaluate only the POD accuracy dependent on the disturbance models. The mean biases and standard deviations (STDs) of the SLR residuals are presented in Tables 6 and 7.

The SLR residuals of the seven-parameter ECOM2 without an a priori model, located in the top row of Fig. 16, show

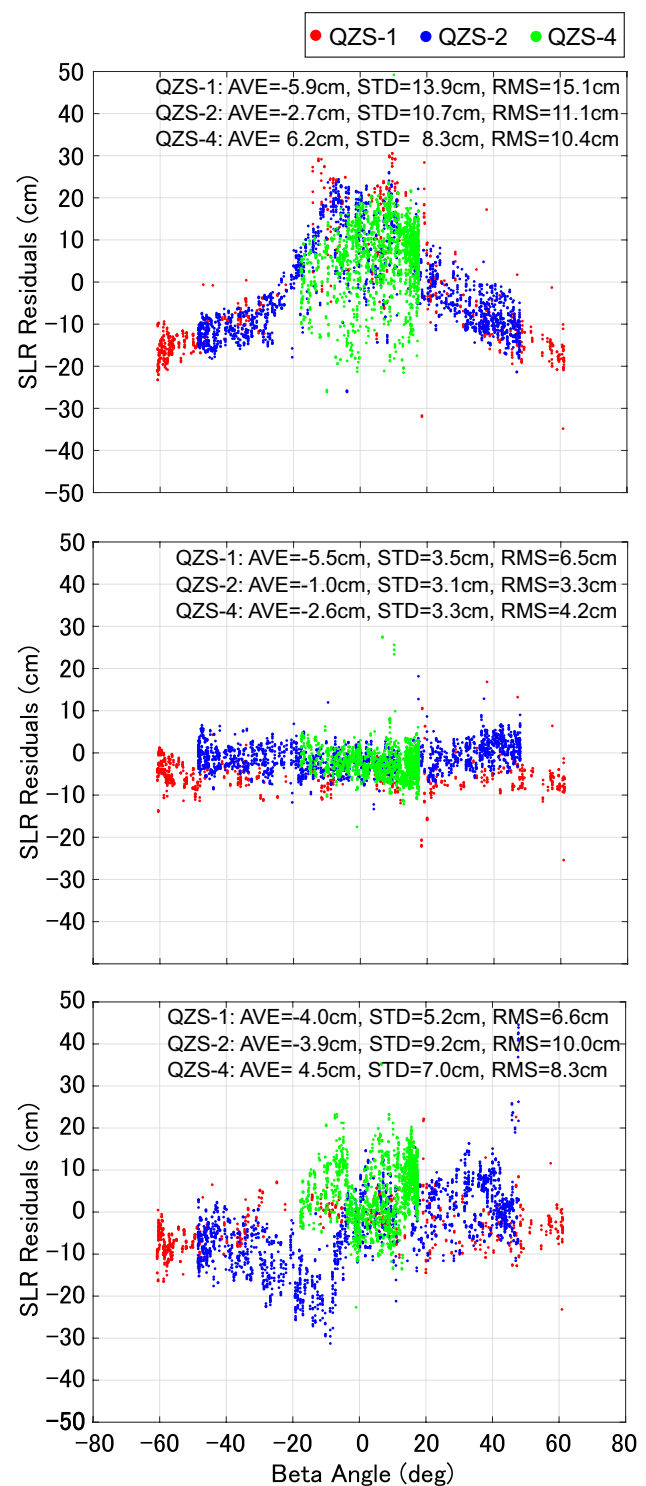


**Fig. 16** SLR residuals of QZSS satellites using different force models. The horizontal axis shows the beta angle. The top panel is obtained by the no a priori model, the middle by our proposed PCGT SRP+TRP model, and the bottom is obtained by the JAXA MGEX products

**Table 6** QZSS SLR residuals (unit cm). Bias and standard deviation (STD) are summarized for each non-gravitational force model we used. Our proposed PCGT SRP+ TRP model provides the best accuracy except for the QZS-1 bias

Solution	QZS-1		QZS-2		QZS-4	
	Bias	STD	Bias	STD	Bias	STD
No a priori model	-5.9	13.8	-2.7	10.7	6.2	8.3
With PCGT SRP+ TRP model	-5.5	3.5	-1.0	3.1	-2.6	3.3
JAXA MGEX products (JXF)	-4.0	5.2	-3.9	9.2	4.5	7.0

**Table 7** QZSS SLR residuals in previous studies (unit cm). Our proposed PCGT SRP+ TRP model also provides the best accuracy except for the QZS-1 bias comparing the previous studies

Previous Study	QZS-1		QZS-2		QZS-4	
	Bias	STD	Bias	STD	Bias	STD
Darugna et al. (2018)	YS: -3.9 ON: -1.9	YS: 5.5 ON: 14.2	-	-	-	-
Yuan et al. (2020) Box-wing-hat model	YS: -4.4 ON: -7.6	YS: 5.6 ON: 13.1	1.2	5.5	3.5	5.3

beta-angle-dependent variation. For the QZS-1 and QZS-2 satellites, which are located in orbital planes with large beta angle variations, the SLR residuals shift in a negative direction during periods of large absolute beta angles, and conversely, the SLR residuals shift in a positive direction during periods when the absolute beta angles are approximately 20 degrees or less. For the QZS-4 satellite, which has a small beta angle variation, a positive offset can be observed during periods when the absolute value of the beta angle is less than 20 degrees. This result suggests that such beta-angle-dependent errors in satellite positions, especially in the radial direction, may not be eliminated by applying only empirical ECOM2 without an a priori model to QZSS satellites in the IGSO. On the other hand, the SLR residuals with the proposed SRP and TRP models show a significant improvement in systematic variation compared with those without a priori models. For the QZS-1, 2, and 4 satellites, the STDs of the SLR residuals with the proposed a priori model are 3.5, 3.1, and 3.3 cm, respectively, which are 75, 71, and 60% smaller than those without the a priori model. In comparison with the SLR residuals of the JAXA's MGEX products, which are tuned with a long-term observation data, as shown in the bottom row of Fig. 16, the bias and STD are also small for all three satellites.

We also compared the SLR residuals obtained by other QZSS analytical models by Darugna et al. (2018) and Yuan et al. (2020). All standard deviations of SLR residuals obtained by the PCGT SRP+ TRP model are smaller than other analytical models. This comparison result shows that our proposed analytical model with high-fidelity satellite information can provide better POD results than other analytical models. The bias error for QZS-1 by the Darugna is smaller than our proposed method. The large SLR bias for

QZS-1 is our problem to solve. As mentioned in the section on SRP parameter estimation, the effect of antenna thrust could cause this error.

### Conclusions

We propose an accurate analytical non-gravitational force model of QZS-1, 2, and 4 for precise orbit determination of these satellites. To construct an accurate disturbance model, we used a high-fidelity satellite geometry model and the thermal information provided by the satellite developer. They are the most detailed design information to be used to construct the analytical solar radiation pressure and thermal radiation pressure models ever for QZSS satellites. We applied the pre-computed geometry tensor method for solar radiation pressure modeling and constructed a simple box-wing-hat thermal radiation pressure model. In particular, this thermal radiation pressure is the first model, which is constructed with realistic temperature information. Based on the analytical model, we also proposed a hybrid model combined with an empirical approach to estimate the ECOM five parameters. The accurate non-gravitational force models were implemented on a precise orbit determination tool called MADOCA, and orbit determination experiments were performed for QZS-1, 2, and 4. Thanks to the tensor approximation, the calculation cost of the proposed method is not high compared to the normal ray-tracing method; thus the proposed method can be worked in the routine orbit determination work with MADOCA. The results show that the hybrid model can improve orbit determination accuracy

compared with previous empirical and analytical approaches without long-term estimation after the launch of these satellites.

The estimated ECOM parameters show that the accuracy of the proposed non-gravitational acceleration model constructed with only such pre-defined information for QZS-2 and 4 is better than  $2 \text{ nm/s}^2$  and for QZS-1 better than  $5 \text{ nm/s}^2$ . Using the proposed model, the standard deviations of the SLR residuals are improved by 75, 71, and 60% for QZS-1, 2, and 4, respectively, using the pure empirical approach without an a priori model. The SLR residuals obtained by the proposed model are more accurate than the current JAXA MGEX products, which are tuned using long-term observation data. The SLR residuals obtained by the proposed model are also more accurate than other previous analytical disturbance models for QZSS satellites. These results demonstrate the importance of the analytical non-gravitational disturbance model with high-fidelity satellite information obtained from the satellite design information by the manufacturer. It is possible to improve precise orbit determination results for other GNSS satellites if high-fidelity geometry and thermal models are published and the proposed methods are applied to these satellites without parameter tuning using long-term observation data.

**Supplementary Information** The online version contains supplementary material available at <https://doi.org/10.1007/s10291-023-01527-0>.

**Acknowledgements** We would like to thank Prof. Minoru Iwata at the Kyushu Institute of Technology for his support in measuring the optical properties. This work was supported by JSPS KAKENHI Grant Number JP17H06615.

**Author contributions** Satoshi Ikari, Takuji Ebinuma, and Shinichi Nakasuka proposed the accurate analytical disturbance modeling method used in the paper. Kyohei Akiyama, Yuki Igarashi, Kaori Kawate, and Toshitaka Sasaki executed the precise orbit determination experiment with MADOCA. Yasuyuki Watanabe prepared the high-fidelity satellite design information used in this study. Satoshi Ikari wrote the main manuscript text, and Kyohei Akiyama wrote the POD Experiment section text. All authors reviewed the manuscript.

**Data availability** We published the force table data obtained by the proposed analytical non-gravitational model for the QZS-1, 2, and 4 satellites. The QZSS satellite orbit determination products with the proposed analytical non-gravitational model are published on the MADOCA Products page (<https://mgmds01.tksc.jaxa.jp/>).

## Declarations

**Competing interests** The authors declare no competing interests.

## References

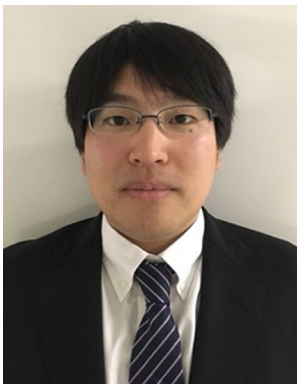
- Arnold D et al (2015) CODE's new solar radiation pressure model for GNSS orbit determination. *J Geod* 89:775–791. <https://doi.org/10.1007/s00190-015-0814-4>
- Beutler G, Brockmann E, Gurtner W, Hugentobler U, Mervart L, Rothacher M (1994) Extended orbit modeling techniques at the CODE processing center of the international GPS Service for Geodynamics (IGS): theory and initial results. *Manuscripta Geod* 19:367–386
- Bhattarai S, Ziebart M, Springer T, Gonzalez F, Tobias G (2022) High-precision physics-based radiation force models for the Galileo spacecraft. *Adv Space Res* 69:4141–4154. <https://doi.org/10.1016/j.asr.2022.04.003>
- Boehm J, Heinkelmann R, Schuh H (2007) Short Note: a global model of pressure and temperature for geodetic applications. *J Geod* 81:679–683. <https://doi.org/10.1007/s00190-007-0135-3>
- Boehm J, Niell A, Tregoning P, Schuh H (2006) Global mapping function (GMF): a NEW empirical mapping function based ON numerical weather model data. *Geophys Res Lett* 33:7. <https://doi.org/10.1029/2005GL025546>
- Cabinet Office (2023) QZSS satellite information (Operational history information). <https://qzss.go.jp/en/technical/qzssinfo/index.html> (Accessed on 23rd March 2023)
- Darugna F, Steigenberger P, Montenbruck O, Casotto S (2018) Ray-tracing solar radiation pressure modeling for QZS-1. *Adv Space Res* 62:935–943. <https://doi.org/10.1016/j.asr.2018.05.036>
- Fliegel HF, Gallini TE (1996) Solar force modeling of block IIR Global Positioning System satellites. *J Spacecraft Rockets* 33:863–866. <https://doi.org/10.2514/3.26851>
- Fliegel HF, Gallini TE, Swift ER (1992) Global Positioning System Radiation Force Model for geodetic applications. *J Geophys Res* 97:559–568. <https://doi.org/10.1029/91JB02564>
- Folkner WM, Williams JG, Boggs DH (2009) The planetary and lunar ephemeris DE 421. *IPN Progress Report:42, 178, 1–34*
- Ikari S, Ebinuma T, Funase R, Nakasuka S (2014) Analytical nonconservative disturbance modeling for QZS-1 precise orbit determination. *Proc. ION GNSS 2014*, Institute of Navigation, Tampa, Florida, USA, Sept 8–12, p 2440–2447
- Ikari S, Tokunaga K, Ito T, Inamori T, Funase R, Nakasuka S (2017) Optical property estimation by pre-computed tensor method for high-fidelity SRP model Proceedings of the 30th ISTS and ISSFD 2017:ISTS-2017-d-2062/ISSFD-2017-062
- Kawate K et al (2023) MADOCA: Japanese precise orbit and clock determination tool for GNSS. *Adv Space Res*. <https://doi.org/10.1016/j.asr.2023.01.060>
- Prange L, Beutler G, Dach R et al (2020) An empirical solar radiation pressure model for satellites moving in the orbit-normal mode. *Adv Space Res*. <https://doi.org/10.1016/j.asr.2019.07.031>
- Milani A, Nobili AM, Farinella P (1987) *Nongravitational perturbations and satellite geodesy*. IOP Publishing Ltd, England
- Montenbruck O, Steigenberger P, Darugna F (2017) Semi-analytical solar radiation pressure modeling for QZS-1 orbit-normal and yaw-steering attitude. *Adv Space Res* 59:2088–2100. <https://doi.org/10.1016/j.asr.2017.01.036>
- Montenbruck O, Steigenberger P, Hugentobler U (2015) Enhanced solar radiation pressure modeling for Galileo satellites. *J Geod* 89:283–297. <https://doi.org/10.1007/s00190-014-0774-0>
- Pavlis NK, Holmes SA, Kenyon SC, Factor JK (2012) The development and evaluation of the earth gravitational model 2008 (EGM2008). *J Geophys Res*. <https://doi.org/10.1029/2011JB008916>
- Pearlman MR, Degnan JJ, Bosworth JM (2002) The international laser ranging service. *Adv Space Res* 30:135–143. [https://doi.org/10.1016/S0273-1177\(02\)00277-6](https://doi.org/10.1016/S0273-1177(02)00277-6)
- Pearlman MR, Noll CE, Pavlis EC, Lemoine FG, Combrink L, Degnan JJ, Kirchner G, Schreiber U (2019) The ILRS: approaching 20 years and planning for the future. *J Geod* 93:2161–2180. <https://doi.org/10.1007/s00190-019-01241-1>
- Petit G, Luzum B (2010) IERS conventions, IERS technical note; No. 36



- Rebischung P (2020) Switch to IGB14 reference frame. IGS-MAIL-7921, Accessed 14 Apr 2020. <https://lists.igs.org/pipermail/igsmail/2020/007917.html>
- Rebischung P, Schmid R (2016) IGS14/igs14.atx: a new framework for the IGS products. <https://mediatum.ub.tum.de/1341338>, AGU Fall Meeting
- Rodriguez-Solano CJ, Hugentobler U, Steigenberger P (2012) Adjustable box-wing model for solar radiation pressure impacting GPS satellites. *Adv Space Res* 49:1113–1128. <https://doi.org/10.1016/j.asr.2012.01.016>
- Saastamoinen J (1972) Atmospheric correction for the troposphere and stratosphere in radio ranging of satellites, the use of artificial satellites for geodesy. *Geophys Monogr Ser* 15:247–251. <https://doi.org/10.1029/GM015p0247>
- Springer TA, Beutler G, Rothacher M (1999) A new solar radiation pressure model for GPS. *Adv Space Res* 23:673–676. [https://doi.org/10.1016/S0273-1177\(99\)00158-1](https://doi.org/10.1016/S0273-1177(99)00158-1)
- Yuan Y, Li X, Zhu Y, Xiong Y, Huang J, Wu J, Li X, Zhang K (2020) Improving QZSS precise orbit determination by considering the solar radiation pressure of the L-band antenna. *GPS Solut*. <https://doi.org/10.1007/s10291-020-0963-7>
- Ziebart M (2001) High precision analytical solar radiation pressure modelling for GNSS spacecraft. University of East London

**Publisher's Note** Springer Nature remains neutral with regard to jurisdictional claims in published maps and institutional affiliations.

Springer Nature or its licensor (e.g. a society or other partner) holds exclusive rights to this article under a publishing agreement with the author(s) or other rightsholder(s); author self-archiving of the accepted manuscript version of this article is solely governed by the terms of such publishing agreement and applicable law.



**Satoshi Ikari** is an assistant professor in the Department of Aeronautics and Astronautics at the University of Tokyo. His research focuses on astrodynamics and the attitudes and orbit control of satellites. In particular, he studies the non-gravitational disturbance modeling for GNSS satellites, the application of formation flying satellites, and the development of microsattellites.



**Kyohei Akiyama** works at Japan Aerospace Exploration Agency (JAXA). He has many years of experience on GNSS as an engineer of flight dynamics since 2011, specifically for the precise orbit determination (POD) using GNSS and SLR measurements. He is currently contributing to improving POD software for GNSS satellites and the conceptual design of Quasi-Zenith Satellite System for the future constellation.



**Yuki Igarashi** is currently an engineer at the Satellite Navigation Unit of Japan Aerospace Exploration Agency (JAXA). His research interests include the POD for navigation satellites, navigation satellite transmitters, and wireless communications applied to satellites and their development.



**Kaori Kawate** is a Japan Aerospace Exploration Agency (JAXA) engineer. She has worked for the operation and promotion of the first Quasi-Zenith satellite (QZS-1) since 2011. She is currently contributing to developing the Multi-GNSS precise orbit determination (POD) software.



**Toshitaka Sasaki** is an engineer in the Satellite Navigation Unit of the Japan Aerospace Exploration Agency (JAXA). His specialties are flight dynamics, satellite attitude dynamics, and satellite navigation technology. He is currently engaged in improving JAXA's precise orbit determination software for GNSS and developing on-board components to improve the performance of the next-generation Quasi-Zenith Satellite System.



**Yasuyuki Watanabe** is an engineer working for Mitsubishi Electric Corporation. He received his bachelor's, master's and doctor's degrees in mechano-informatics from the University of Tokyo. His current work is in the field of spacecraft dynamics and GNC design.



**Takuji Ebinuma** is a professor of Astronautics and Aeronautics at Chubu University, Japan. He earned his doctoral degree in aerospace engineering from the University of Texas at Austin. His research primarily focuses on the space applications of GNSS. He is also the creator of GPS-SDR-SIM, an open-source GPS signal simulator widely utilized in academic and research communities.



**Shinichi Nakasuka** graduated from the Graduate School of Engineering at the University of Tokyo and received a Ph.D. in 1988. He has been working for the Department of Aeronautics and Astronautics, University of Tokyo as a lecturer and associate professor and became a full professor in 2004. His major research areas include micro/nano/pico-satellites, autonomy and intelligence for space systems, novel space systems, and guidance, navigation and control of spacecraft.